crystals

MDPI

Article

Indium Ammoniates from Ammonothermal Synthesis: $InAlF_6(NH_3)_2$, $[In(NH_3)_6][AlF_6]$, and $[In_2F(NH_3)_{10}]_2[SiF_6]_5 \cdot 2\ NH_3$

Peter Becker, Toni Boris Cekovski and Rainer Niewa *

Institute of Inorganic Chemistry, University of Stuttgart, Pfaffenwaldring 55, 70569 Stuttgart, Germany; peter.becker@iac.uni-stuttgart.de (P.B.); toni.cekovski@web.de (T.B.C.)
* Correspondence: rainer.niewa@iac.uni-stuttgart.de

Abstract: The ammonothermal synthesis of three ammoniates of indium, namely $InAlF_6(NH_3)_2$, $[In(NH_3)_6][AlF_6]$, and $[In_2F(NH_3)_{10}]_2[SiF_6]_5 \cdot 2\ NH_3$ was successful from near-ammononeutral conditions in the presence of fluoride ions. Initially, all these compounds were obtained upon corrosion of the applied liner and crucible material Si_3N_4, which also contains small amounts of aluminum. The syntheses were performed in supercritical ammonia (T = 753 K, p up to 307 MPa). The crystal structures were solved and refined from single crystal X-ray diffraction intensity data. $InAlF_6(NH_3)_2$ crystallizes as a typical layer-type structure with corner-sharing $[InF_4(NH_3)_2]^-$ and $[AlF_6]^{3-}$ octahedra. $[In(NH_3)_6][AlF_6]$ features isolated $[In(NH_3)_6]^{3+}$ and $[AlF_6]^{3-}$ octahedra. The crystal structure of $[In_2F(NH_3)_{10}]_2[SiF_6]_5 \cdot 2\ NH_3$ contains $[(NH_3)_5In–F–In(NH_3)_5]^{5+}$ octahedra doubles next to $[SiF_6]^{2-}$ octahedra and ammonia molecules. All intermediates have strong hydrogen bonding systems. The results from vibrational spectroscopy are reported.

Keywords: indium nitride; ammonothermal synthesis; intermediates; ammoniates; fluorides

Citation: Becker, P.; Cekovski, T.B.; Niewa, R. Indium Ammoniates from Ammonothermal Synthesis: $InAlF_6(NH_3)_2$, $[In(NH_3)_6][AlF_6]$, and $[In_2F(NH_3)_{10}]_2[SiF_6]_5 \cdot 2\ NH_3$. *Crystals* **2021**, *11*, 679. https://doi.org/10.3390/cryst11060679

Academic Editors: Devki N. Talwar and Sudhiranjan Tripathy

Received: 12 May 2021
Accepted: 9 June 2021
Published: 13 June 2021

1. Introduction

Huge efforts into the investigation of group III nitrides have been made because of their wide application in electronic devices, such as light-emitting diodes and lasers [1]. The wide variety in the band gaps of the binary nitrides AlN (6.2 eV) [2], GaN (3.4 eV) [3], and InN (0.7–1.9 eV) [4–6], as well as solid solutions thereof, predestines these materials for such applications, although the synthesis of high quality material remains challenging. The ammonothermal synthesis route is especially useful for the synthesis of high-quality free-standing crystals of group III nitrides [7–10]. These materials can be employed, for instance, as substrates in hydride vapor phase epitaxy (HVPE), which enables fast growth rates and high purity coupled with high structural quality [11].

The crystal growth of indium nitride is especially challenging due to its labile In–N bond, which is expressed in the low enthalpy of formation [12]. With the ammonothermal synthesis, it was demonstrated that it is possible to synthesize InN crystals with sizes in the micrometer range [13]. During such reactions, so-called mineralizers are used in order to enhance the solubility of the starting materials. In ammonoacidic crystal growth, typically ammonium or metal halides are utilized as mineralizers, while in ammonobasic crystal growth, alkali metals, their amides, or azides come into use. Since InN is highly corrosive against nickel-based alloys, which are typically used for ammonothermal syntheses, ceramic liners from Si_3N_4 or BN are employed to protect the autoclave [14].

Since the chemistry of ammonothermal crystal growth of InN is only scarcely understood, we are particularly interested in the soluble intermediates that occur during the process. For instance, the dissolved intermediates can lead to the crystallization of solid amides or ammoniates, if appropriate conditions are chosen. Only a handful indium ammoniates and amides are known. Purdy synthesized $In(NH_3)_3$, along with other indium amides and nitrides [15]. Ketchum et al. were successful in synthesizing $InF_2(NH_2)(NH_3)$ [16]. Bremm et al. published the crystal structure of $InCl_3(NH_3)_3 = [In(NH_3)_4Cl_2][In(NH_3)_2Cl_4]$ [17]. Recently, we were able

to characterize the compounds $[In(NH_3)_5Cl]Cl_2$ and $InF_2(NH_2)$ [18]. With the synthesis and characterization of $InAlF_6(NH_3)_2$, $[In(NH_3)_6][AlF_6]$, and $[In_2F(NH_3)_{10}]_2[SiF_6]_5 \cdot 2\ NH_3$, we expand the scarce state of knowledge on indium ammoniates formed under near-ammononeutral conditions involving fluoride ions in the mineralizer system. Furthermore, we demonstrate how corrosion products stemming from the liner material can take part in the transport mechanisms of ammonothermal InN synthesis. Finally, knowledge on simultaneously dissolved group III metals in ammonothermal systems may lead the way towards the crystallization of solid solutions of their nitrides as well as intentionally doped nitride semiconductors.

2. Materials and Methods

The general approach of synthesizing intermediates in near-ammononeutral InN synthesis has already been discussed in the literature [18]. We chose reaction conditions similar to the ammonothermal InN crystal growth [13], thus using custom-made 97 mL autoclaves from nickel-based alloy with an internal Si_3N_4 liner, which prevents the autoclave from corrosion [19,20]. As reactants, InF_3 and KNH_2 were used in a molar ratio of 1:3. In order to avoid solid-state reactions of these starting materials, we used small crucibles from Si_3N_4, which fit into the Si_3N_4 liners (air-pressure sintered silicon nitride, Ingenieurkeramik, a QSIL company, Frankenblick, Germany). The InF_3 was placed within the Si_3N_4 liner, and the KNH_2 in the crucible. The crucible was equipped with a cap with a small hole, which reduced the diffusion rate of the well-soluble mineralizer (KNH_2) into the solution.

All preparative work was done in an argon-filled glovebox with $p(O_2) < 0.1$ ppm (MBRAUN Inertgas-Systeme, Garching, Germany) because of moisture sensitivity of the products and reactants. The ammonia was condensed into the autoclave by cooling in an ethanol/dry ice bath. The amount of condensed ammonia was monitored with a self-made Tensi-Eudiometer, which was designed as described by Hüttig [21]. The reactions were carried out in a vertical tubular furnace, LOBA 1200-60-400-1 OW (HTM Reetz, Berlin, Germany). The use of a one-heating zone furnace results in a temperature gradient from the bottom part of the autoclave within the furnace (hot zone) to its top part poking out (cold zone). The chemical transport reaction was therefore dominated by convection [22,23]. The pressures were monitored with a pressure transmitter HBM P2VA2 and a digital indicator DA 2510 (Hottinger Brüel & Kjaer, Darmstadt, Germany).

$InAlF_6(NH_3)_2$ was synthesized in a slightly ammonobasic milieu, starting from 1.46 mmol InF_3 and KNH_2 in a molar ratio of $n(InF_3)/n(KNH_2) = 1:3.12$. The autoclave was filled with 19.1 g ammonia. The pressure was not monitored in this experiment. $[In(NH_3)_6][AlF_6]$ was synthesized in an ammononeutral milieu, starting from 0.73 mmol InF_3 together with Al, NH_4F, and KNH_2 in a molar ratio of $n(InF_3)/n(Al)/\ n(NH_4F)/n(KNH_2) = 1:1:3:6$. The InF_3, Al, and NH_4F were placed in the liner, and the KNH_2 was placed in the crucible. The autoclave was filled with 20.8 g ammonia. It reached a maximum pressure of 307.3 MPa. $[In_2F(NH_3)_{10}]_2[SiF_6]_5 \cdot 2\ NH_3$ was synthesized in a near ammononeutral milieu, starting from 0.73 mmol InF_3 together with Ga, NH_4F, and KNH_2 in a molar ratio of $n(InF_3)/n(Ga)/n(NH_4F)/n(KNH_2) = 1:1:3:6$. The InF_3, Ga, and NH_4F were placed in the liner, and the KNH_2 in the crucible. The autoclave was filled with 19.7 g ammonia. The pressure was not monitored in this experiment. For all syntheses, the autoclaves were heated to 753 K with a heating rate of 90.8 $K \cdot h^{-1}$. The autoclaves remained at this temperature for 60 h and were subsequently cooled to room temperature with a cooling rate of 90.8 $K \cdot h^{-1}$.

InF_3 (Alfa Aesar, Thermo Fisher, Kandel, Germany, 99.95% metal basis, anhydrous), Al (Alfa Aesar, 99.97% metal basis), Ga (Sigma Aldrich, Merck, Darmstadt, Germany, 99.99999% metals basis), and NH_4F (Sigma Aldrich, >99.99%) were used. The KNH_2 was self-made, synthesized from potassium (Sigma Aldrich, 98 %) reacting with ammonia at 373 K for 24 h.

Single crystal X-ray diffraction of $InAlF_6(NH_3)_2$ and $[In_2F(NH_3)_{10}]_2[SiF_6]_5 \cdot 2\ NH_3$ was performed on a Stoe & Cie Stadivari (Darmstadt, Germany) four-circle diffractometer, and the diffraction experiment on $[In(NH_3)_6][AlF_6]$ on a κ-CCD (Bruker Cooperation, Billerica,

MA, USA). All crystal structures were solved and refined with the SHELX-2013 software package [24,25]. Powder X-ray diffraction experiments (PXRD) were carried out on a Stoe & Cie Stadi-P equipped with a Dectris Mythen 1K detector, using Mo-$K\alpha_1$ radiation.

Single crystal Raman spectra were obtained on a XploRa Raman spectrometer (Horiba Europe, Oberursel, Germany) with a confocal polarization microscope (Olympus BX51, Olympus Europa, Hamburg, Germany). For data collection of both single crystal X-ray diffraction and Raman spectroscopy, selected crystals were sealed in glass capillaries under argon atmosphere. Infrared spectroscopy measuring on powder samples was performed under nitrogen atmosphere on a Nicolet iS5 FTIR (Thermo Fisher Scientific, Waltham, MA, USA).

Wavelength dispersive X-ray spectroscopy was performed on a Cameca SX-100 microprobe analyzer (CAMECA, Société par Actions Simplifiée (SAS), Gennevilliers, France) equipped with 5 wavelength dispersive X-ray spectrometers. The samples were placed on an adhesive carbon plate and sputtered with gold. The presence of all constituting elements heavier than nitrogen in the respective product crystals was proven via microprobe analysis. The silicon nitride liner material was investigated particularly with the presence of aluminum employing the Al-K_α line with an accelerating voltage of 15 kV and a beam current of 20 nA.

3. Results

Intermediates, which form during near-ammononeutral InN synthesis can be obtained by reacting indium trihalides together with three molar equivalents of an alkali metal amide (typically KNH_2). Since indium forms intermetallic phases with many metals and alloy constituents, it is necessary to protect the autoclave material from direct contact with the reactants. To protect the autoclave material from corrosion, we typically use liners made from Si_3N_4 [14]. Additionally, we spatially separated the reactants in order to prevent solid-state reactions, rather than reactions of dissolved materials. This synthetic approach was already successful for the synthesis of $[In(NH_3)_5Cl]Cl_2$ and $InF_2(NH_2)$ [18]. If the reaction media is sufficiently aggressive, which is the case with the use of fluorides as a constituent of the mineralizer system, we have frequently observed attacks on the ceramic liner and crucible materials. Within the presented work, this equally concerns the formation of silicon compounds by the partial dissolution of the used Si_3N_4 and further components of this material, such as small amounts of aluminum used as a sintering aid during production. According to the producer, the material contains about 4 wt.% aluminum oxide. The presence of aluminum in the Si_3N_4 material was proven by wavelength dispersive X-ray spectroscopy (WDS).

$InAlF_6(NH_3)_2$ forms as a corrosion product from the liner material when indium trifluoride is used as the starting material, alongside the dominating compound $InF_2(NH_2)$ [18]. These two products were isolated from the bottom of the liner, which represents the hotter zone of the reaction container, implying a retrograde solubility, that is, lower solubility at higher temperatures. For a targeted synthesis of $InAlF_6(NH_3)_2$ we used InF_3 together with Al, NH_4F, and KNH_2 in a molar ratio of $n(InF_3)/n(Al)/n(NH_4F)/n(KNH_2)$ = 1:1:3:6. However, instead of $InAlF_6(NH_3)_2$, we isolated $[In(NH_3)_6][AlF_6]$ from the hot temperature zone of the reaction vessel, forming as colorless crystals with a cubic habitus. A PXRD measurement revealed the presence of this title compound next to indium metal, KF, and small amounts of further unknown impurities. The powder pattern can be found in Figure S1 in the Supplementary Materials. Furthermore, $[In_2F(NH_3)_{10}]_2[SiF_6]_5 \cdot 2\,NH_3$, as a further corrosion product of the liner material, was observed in an experiment employing InF_3 together with Ga, NH_4F, and KNH_2 in a molar ratio of $n(InF_3)/n(Ga)/n(NH_4F)/n(KNH_2)$ = 1:1:3:6. The synthesis aimed at a possible bimetallic intermediate in the system In/Ga. Presumably due to the low solubility of Ga within the applied reaction conditions and mineralizer system, the title compound formed as a corrosion product of the liner material instead. Colorless crystals of this title compound were isolated from the hot temperature zone of the reaction vessel. The presence of all constituting elements heavier than nitrogen was proven via microprobe analysis on the respective crystals.

Selected crystallographic parameters and refinement data of all three compounds are presented in Tables 1 and 2.

Table 1. Selected crystallographic parameters and refinement data of $InAlF_6(NH_3)_2$ and $[In(NH_3)_6][AlF_6]$.

Composition	**$InAlF_6(NH_3)_2$**	**$[In(NH_3)_6][AlF_6]$**
Crystal system	Monoclinic	Cubic
Space group	$C2/m$	$Pa\bar{3}$
a/pm	1056.77(9)	1012.55(3)
b/pm	560.96(5)	
c/pm	488.01(4)	
β/°	92.346(7)	
Z	2	4
Density (calculated)/g · cm^{-3}	3.332	2.291
Volume/10^6 pm^3	288.91(4)	1038.12(9)
Index ranges hkl	±15; ±8; ±7	$-12 \leq h \leq 11$ $-13 \leq k \leq 12$ $-13 \leq l \leq 12$
$2\theta_{max}$/°	63.72	54.81
$F(000)$	272	704
T/K	100	293
Diffractometer	STOE & Cie STADIVARI	κ-CCD (Bruker-Nonius)
μ(Mo-K$_{\alpha 1}$)/mm^{-1}	4.30	2.43
Measured reflections/ sym. independent	9902/531	9000/398
R_{int}/R_σ	0.0322/0.0129	0.0555/0.0162
R_1 with $\lvert F_o\rvert > 4\sigma(F_o)$	0.0133	0.0180
$R_1/wR_2/GooF$	0.0139/0.0326/1.139	0.0256/0.0471/1.130
Remaining electron density/10^6 pm^{-3}	0.68/−0.63	0.37/−0.28

Table 2. Selected crystallographic parameters and refinement data of $[In_2F(NH_3)_{10}]_2[SiF_6]_5 \cdot 2\ NH_3$ at two different temperatures, collected on the identical single crystal. The positions of the hydrogen atoms could not be refined for the measurement at 293 K.

Composition	**$[In_2F(NH_3)_{10}]_2[SiF_6]_5 \cdot 2\ NH_3$**	
Crystal system	Orthorhombic	Orthorhombic
Space group	*Pnma*	*Pnma*
a/pm	1407.11(4)	1413.02(4)
b/pm	2527.15(6)	2534.31(6)
c/pm	1322.65(5)	1326.37(5)
Z	4	4
Density (calculated)/g · cm^{-3}	2.226	2.205
Volume/10^6 pm^3	4703.3(3)	4749.8(3)
Index ranges *hkl*	$-18 \leq h \leq 18$ $-32 \leq k \leq 33$ $-17 \leq l \leq 7$	$-18 \leq h \leq 18$ $-33 \leq k \leq 33$ $-17 \leq l \leq 17$
$2\theta_{max}$/°	55.75	55.75
F(000)	3072	3072
T/K	100	293
Diffractometer	STOE & Cie STADIVARI	STOE & Cie STADIVARI
μ(Mo-K$_{\alpha 1}$)/mm^{-1}	2.22	2.21
Measured reflections/ sym. independent	39,019/5733	35,630/5795
R_{int}/R_σ	0.0682/0.0472	0.0479/0.0382
R_1 with $\|F_o\| > 4\sigma(F_o)$	0.0518	0.0484
$R_1/wR_2/GooF$	0.0736/0.1466/1.034	0.0742/0.1392/1.052
Remaining electron density/10^6 pm^{-3}	1.63/−1.64	1.14/−1.00

3.1. $InAlF_6(NH_3)_2$

3.1.1. Crystal Structure

$InAlF_6(NH_3)_2$ crystallizes in the monoclinic space group C2/m. For selected crystal structure parameters and refinement data, see Table 1. The atomic parameters and isotropic displacement parameters are presented in Table 3; for the anisotropic displacement parameters, check Table S1 in the Supplementary Materials. For the interatomic distances and angles, see Table 4.

Table 3. Fractional atomic coordinates and isotropic displacement parameters (in 10^4 pm^2) of $InAlF_6(NH_3)_2$.

Atom	**Site**	**x/a**	**y/b**	**z/c**	**U_{eq}**
In	2a	0	0	0	0.00640(8)
Al	2d	½	0	½	0.00346(15)
F(1)	8j	0.43653(8)	0.23377(17)	0.71805(18)	0.01012(18)
F(2)	4i	0.35497(13)	0	0.3059(3)	0.0099(2)
N	4i	0.18306(18)	0	0.8286(4)	0.0095(3)
H(1)	8j	0.192(2)	0.116(4)	0.721(5)	0.011(5)
H(2)	4i	0.245(4)	0	0.959(8)	0.020(9)

Table 4. Selected interatomic distances (in pm) and angles (in deg.) in $InAlF_6(NH_3)_2$.

	Distance		**Distance**
In–F(1)	212.03(9) 4×	Al–F(1)	183.27(9) 4×
In–N	213.88(19) 2×	Al–F(2)	176.84(14) 2×
	Angle		**Angle**
F(1)–In–F(1)	89.50(5)	F(1)–Al–F(1)	88.68(6)
F(1)–In–F(1)	90.50(5)	F(1)–Al–F(1)	91.32(6)
F(1)–In–F(1)	180	F(1)–Al–F(1)	180
F(1)–In–N	89.23(4)	F(1)–Al–F(2)	88.92(4)
F(1)–In–N	90.77(4)	F(1)–Al–F(2)	91.08(4)
N–In–N	180	F(2)–Al–F(2)	180
		In–F(1)–Al	140.06(5)

The crystal structure of $InAlF_6(NH_3)_2$ features one crystallographic site for indium, one for aluminum, two for fluorine, and one for nitrogen. The positions of the two crystallographically distinct hydrogen sites were taken from the difference Fourier map and refined without application of any constraints or restraints. The crystal structure can be understood as the stacking of layers of octahedrally coordinated indium and aluminum, as depicted in in Figure 1. Within these layers, vertex-sharing $InF_4(NH_3)_2$ and AlF_6 octahedra are alternatingly arranged in a checkerboard manner (Figure 2). The interconnection of these octahedra is realized via the ligand F(1), while ammonia and F(2) terminate the layers at indium and aluminum atoms, respectively. This arrangement can be conveniently described with the Niggli formula $^2_\infty\{\left[In(NH_3)^t_{2/1}F(1)^c_{4/2}\right]\left[AlF(2)^t_{2/1}F(1)^c_{4/2}\right]\}$. These layers of vertex-sharing octahedra are stacked along the *a*-axis in the sequence *AB*, such that the terminal ligands are pointing into empty spaces of the neighboring layers. Interconnection between the layers is realized by N–H···F(2) hydrogen bonds (compare Figure 3a).

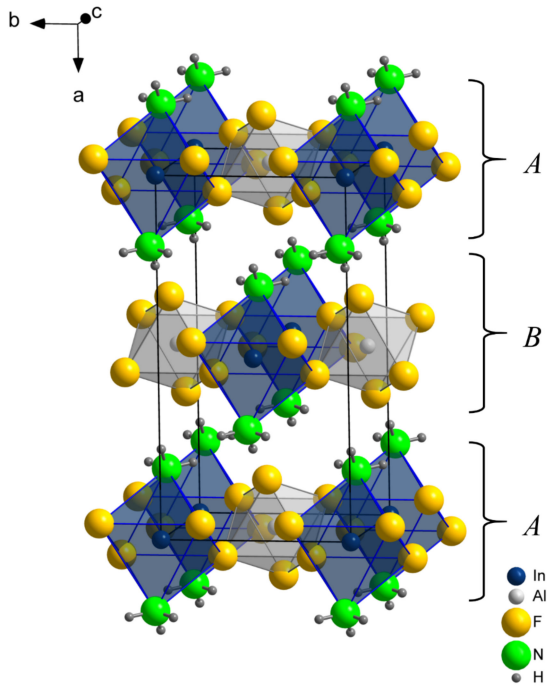

Figure 1. Section of the crystal structure of $InAlF_6(NH_3)_2$ with indication of the layer-type motif. The unit cell is given.

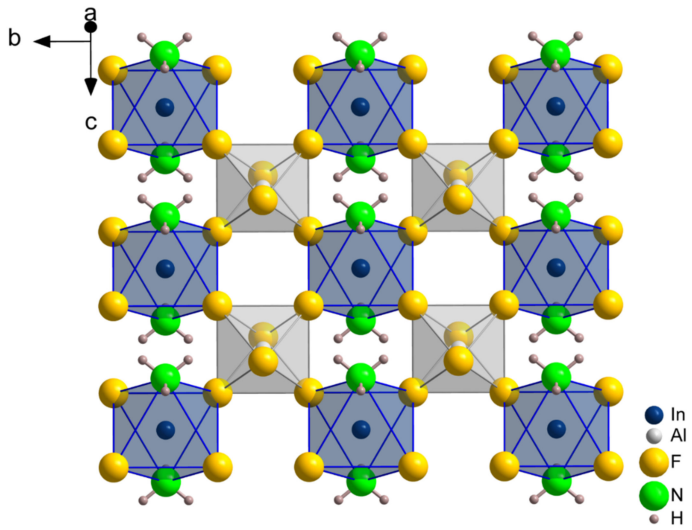

Figure 2. Section of the crystal structure of $InAlF_6(NH_3)_2$ showing one layer of fluorine-sharing octahedra within the (100) plane.

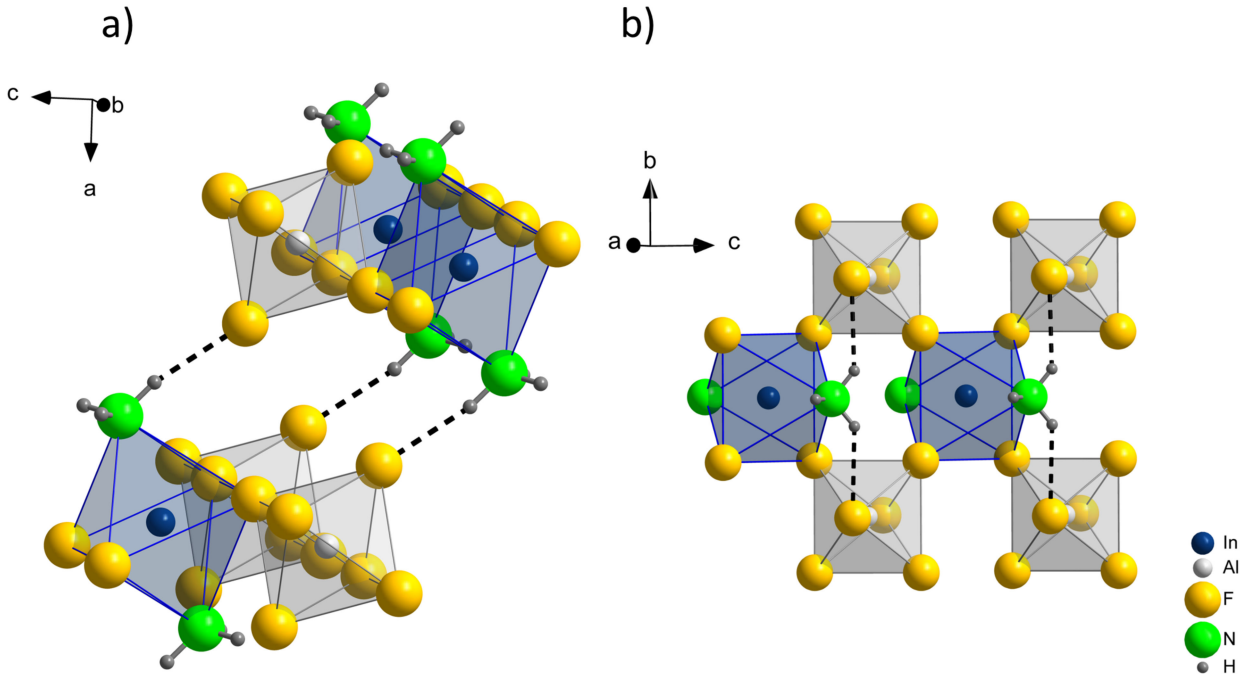

Figure 3. Arrangements of the different hydrogen bonds in $InAlF_6(NH_3)_2$, (**a**) N–H(2)···(2) interconnecting neighboring layers, (**b**) N–H(1)···F(2) located within the layers.

The interatomic distance In–F(1) with 212 pm is slightly shorter than the In–N distance with 214 pm. The Al−F(2) distance of 177 pm is noticeably shorter than the Al–F(1) distance with 183 pm, which is due to the lower coordination number of the terminal ligands F(2) compared to the ligands F(1) realizing the corner-sharing. For $InF_2(NH_2)(NH_3)$, Ketchum et al. reported an In–F distance of 219–220 pm for edged-sharing fluoride ligands [16], expectedly longer than the In–F distance in $InAlF_6(NH_3)_2$. However, the In−(NH_3) distance in $InF_2(NH_2)(NH_3)$ with 223 pm is noticeably longer than the In–N distance in $InAlF_6(NH_3)_2$. For comparison, in $InF_2(NH_2)$, the In–F distance of the corner-sharing fluoride ligand is found to be 212 pm, and the In–N distances around 214–216 pm, quite similar to the respective distances in $InAlF_6(NH_3)_2$ [18]. The In–F(1)–Al angle in the title compound with 140° indicates the octahedra being tilted with respect to each other.

The compound $InAlF_6(NH_3)_2$ features two different hydrogen bonds: N–H(1)···F(2) and N–H(2)···F(2). While N–H(2)···F(2) is responsible for the interconnection between the above discussed layers, N–H(1)···F(2) strengthens the interactions within these layers. Both hydrogen bonds are illustrated in Figure 3. The distances and angles of these hydrogen bonds are presented in Table 5. Strong D–H···A hydrogen bonds are expected, if the donor–acceptor distance is shorter than the sum of the van der Waals radii, which is 302 pm for nitrogen and fluorine [26,27]. Furthermore, the angle ∡(DHA) should be close to 180°. Both hydrogen bonds, N–H(1)···F(2) and N–H(1)···F(2), feature N···F(2) distances shorter than the sum of the van der Waals radii of N and F, and can be classified as strong in this regard. However, with ∡(N–H(1)···F(2)) = 139° and ∡(N–H(2)···F(2)) = 168°, the ∡(DHA) angles differ significantly, which indicates a stronger hydrogen bonding between rather than within the layers, possibly due to geometric restrictions. This is also supported by the single crystal Raman spectrum (compare Figure 4), where strong hydrogen bonds are expected to shift the N–H stretching vibrations to lower frequencies [28].

Table 5. Interatomic distances (in pm) and angles (in deg.) of the hydrogen bonds in $InAlF_6(NH_3)_2$.

	D–H	A	H···A	D···A	∡(DHA)
N–H(1)	85(2)	F(2)	221(2)	290.35(7)	139(2)
N–H(2)	89(4)	F(2)	202(4)	289.5(2)	168(4)

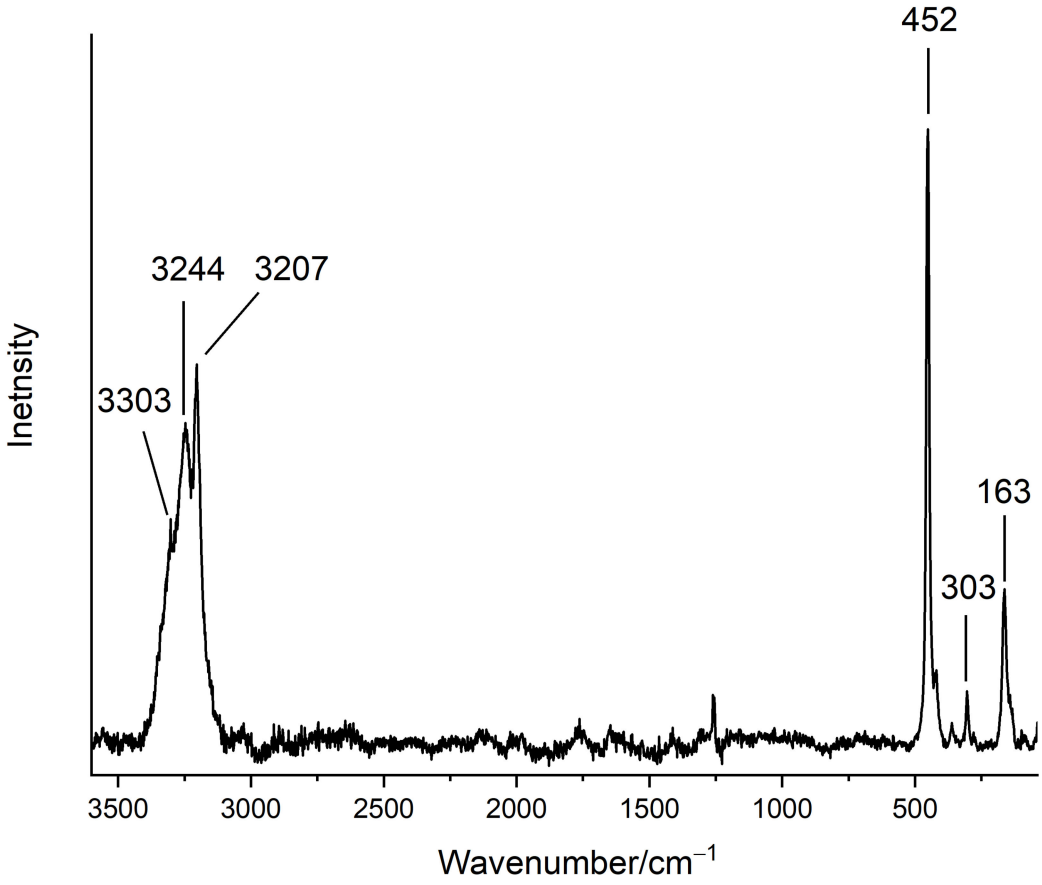

Figure 4. Single crystal Raman spectrum taken on $InAlF_6(NH_3)_2$, excitation wavelength: 532 nm.

The compound $Ga(NH_3)(NH_2)F_2$ crystallizes isostructural to $InAlF_6(NH_3)_2$ with very similar cell parameters [29]. In the crystal structure of this compound, gallium replaces indium and aluminum in $InAlF_6(NH_3)_2$, while ammonia and amide ions occupy the positions of F(2) and NH_3 in the title compound, respectively. Merely the F(1) site of

$InAlF_6(NH_3)_2$ is occupied by an equivalent fluoride ion in $Ga(NH_3)(NH_2)F_2$. The interatomic distances of the coordinating ligands in $Ga(NH_3)(NH_2)F_2$ are d(Ga–F) = 194 and 195 pm, d(Ga–NH_2) and d(Ga–NH_3) = 190 pm. Roos et al. identified the positions of the hydrogen atoms from the difference Fourier map and argued that the presence of amide can be confirmed by Raman spectroscopy. An observed weak signal at 1541 cm^{-1} was assigned to a N–H deformation vibration mode of the amide ligand. An arrangement of the ligands in $InAlF_6(NH_3)_2$ with analogous location of ammonia molecules, amide, and fluoride ions, that is, replacing NH_3 by NH_{2-} in the surroundings of In and NH_3 by F^- in the environment of Al, which would mean $^2_\infty\{[In(NH_2)^t_{2/1}F(1)^c_{4/2}][Al(NH_3)^t_{2/1}F(1)^c_{4/2}]\}$ is unlikely according to the following arguments. Firstly, according to the Hard and Soft Acids and Bases (HSAB) concept, the harder fluoride ligand is expected to preferentially bind to the harder aluminum cation. Secondly, the Al–F(2) distance with 183 pm appears to be too short for an Al–NH_3 bond, which is typically in the range of 192–205 pm [16,30–33]. Furthermore, we find no indication from the crystal structure refinement or spectroscopy for this alternative arrangement.

3.1.2. Raman Spectroscopy

Raman spectroscopy was performed on the identical crystal, which was used for the X-ray diffraction experiment for structure determination. Vibrational spectroscopy is especially helpful to identify stretching and deformation vibrations of the ammine and fluoride ligands $\nu(NH_3)$, ν(In–N,F), ν(Al–F) and $\delta(NH_3)$, δ(N,F–In–N,F), δ(F–Al–F), and thus, gives helpful information about the constitution of the compound. Due to the limited size of the crystal, the spectrum shows only weak signals. Multiple signals of the ν(N–H) stretching vibrations can be observed in the range of 3207–3303 cm^{-1}. In gaseous ammonia, only two signals for the symmetric and antisymmetric stretching vibrations can be observed at 3337 cm^{-1} and 3450 cm^{-1}. The occurrence of multiple signals indicates the presence of at least two crystallographically distinct hydrogen atoms, while the shift to lower frequencies is an effect of different involvement into hydrogen bonding, which weakens the N–H bonds [28]. Signals for N–H stretching vibrations in the above-mentioned energy range are typical for indium and gallium ammoniates. $[In(NH_3)_5Cl]Cl_2$ shows signals at 3151–3311 cm^{-1} [18]. In $Ga(NH_3)_3F_3$, they can be observed at 3182–3315 cm^{-1} [34], in $Ga(NH_3)(NH_2)F_2$ at 2961–3373 cm^{-1} [29].

$\delta(NH_3)$ deformation modes would be expected to occur in the range of 1300–1700 cm^{-1}, but are not observed because of the low intensities of these signals. The signals in the range of 100–500 cm^{-1} can be assigned to the ν(In–N), ν(In–F), ν(Al–F) and δ(N,F–In–N,F), δ(F–Al–F) stretching and deformation vibrations.

3.2. $[In(NH_3)_6][AlF_6]$

3.2.1. Crystal Structure

Hexaammineindium (III) aluminum hexafluoride $[In(NH_3)_6][AlF_6]$ crystallizes in the cubic space group $Pa\bar{3}$ with a lattice parameter of a = 1012.55(3) pm. Selected crystallographic data and refinement parameters are summarized in Table 1, and the fractional atomic coordinates and isotropic displacement parameters can be found in Table 6. For anisotropic displacement parameters, compare Table S2 in the Supplementary Materials. The crystal structure features one crystallographic site for indium, aluminum, nitrogen, and fluorine each, and three symmetry-independent hydrogen atoms. The positions of the hydrogen atoms were taken and refined from the difference Fourier map without application of any constraints or restraints. It consists of isolated $[In(NH_3)_6]^{3+}$ and $[AlF_6]^{3-}$ octahedra, which are interconnected via a N–H···F hydrogen bonding network. The In–N and Al–F distances refine to 224.1(2) pm and 181.3(1) pm, respectively. Focusing on the centers of gravity of the octahedra, the crystal structure can be described as a hierarchical variant of the NaCl structure type. A section of the crystal structure and a reduced variant, only showing aluminum and indium, is depicted in Figure 5.

Table 6. Fractional atomic coordinates and isotropic displacement parameters (in 10^4 pm^2) of $[In(NH_3)_6][AlF_6]$.

Atom	Site	x/a	y/b	z/c	U_{eq}
In	4a	0	0	0	0.01843(18)
Al	4b	0	½	0	0.0147(3)
F	24d	0.39758(10)	0.13497(10)	0.05778(10)	0.0301(3)
N	24d	0.34899(17)	0.41918(19)	0.14022(17)	0.0276(4)
H(1)	24d	0.355(2)	0.327(3)	0.131(2)	0.054(8)
H(2)	24d	0.262(3)	0.429(2)	0.124(2)	0.052(7)
H(3)	24d	0.366(2)	0.441(2)	0.215(2)	0.055(8)

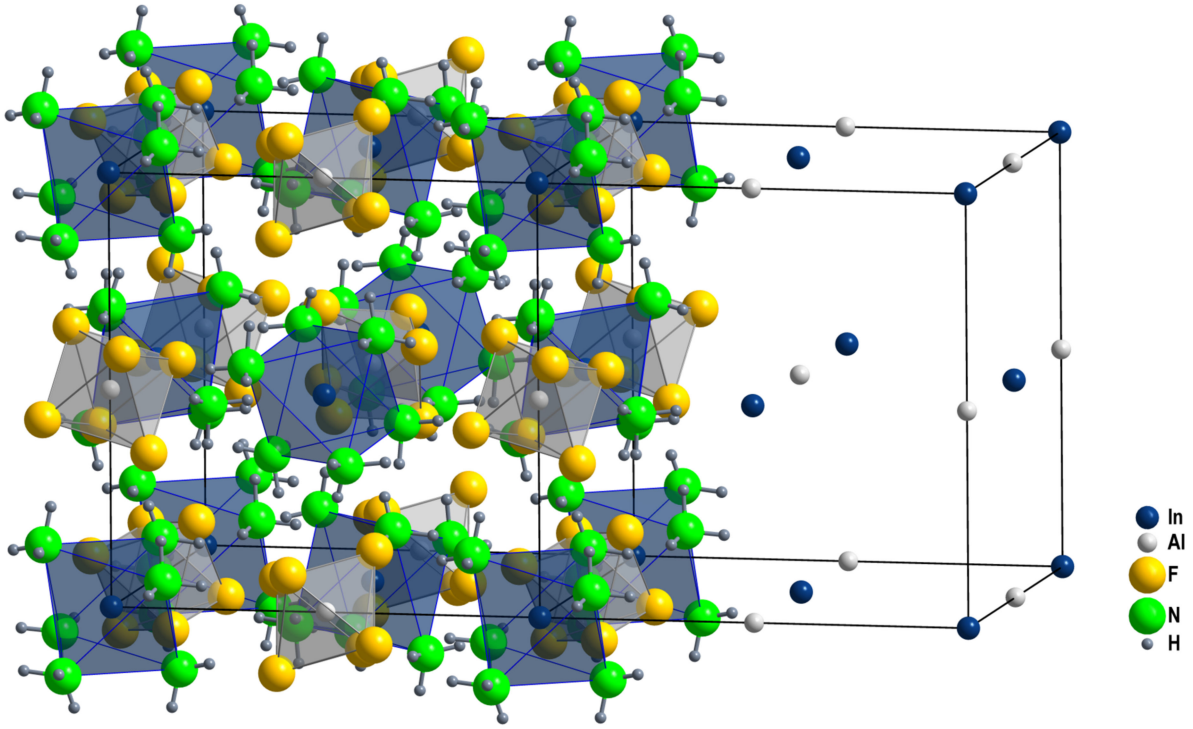

Figure 5. Section of the crystal structure of $[In(NH_3)_6][AlF_6]$ with indicated unit cells on the right, reduced to the central In and Al atoms illustrating the NaCl structure-type motif.

Isotypes with the compositions $[M(NH_3)_6][M'F_6]$, M = Co, Cr and M' = Al, Ga, In, Sc, Ti, V, Cr, Mn, and Fe, as well as $[Rh(NH_3)_6][GaF_6]$, $[Rh(NH_3)_6][MnF_6]$, and $[Rh(NH_3)_6][ScF_6]$ have been previously synthesized by Weighardt et al. by adding a hot, aqueous solution of $[M(NH_3)_6]Cl_3$ to a hot solution of M' in hydrofluoric acid [35–37]. Furthermore, Subramanian et al. were able to synthesize $[Ru(NH_3)_6][M'F_6]$ (M' = Al, Ga, In, Sc, V, Cr, and Fe) by adding HF to an aqueous solution of $[Ru(NH_3)_6]Cl_3$ and an M' metal salt [38]. $[Ru(NH_3)_6][AlF_6]$ is the only hexafluoridoaluminate of this type, of which comprehensive crystal structure data have been published. Compared to $[In(NH_3)_6][AlF_6]$, the interatomic distances of aluminum and fluorine, 183 pm in $[Ru(NH_3)_6][AlF_6]$, are quite similar. The Ru–N distance with 208 pm is noticeably shorter than the In–N distance, which is probably due to the smaller ionic radius of Ru^{3+} compared to In^{3+} in a six-fold coordination [39].

All hydrogen atoms and fluoride ions in $[In(NH_3)_6][AlF_6]$ are involved in hydrogen bonds. Each hydrogen atom of the ammonia ligand connects to a fluoride ligand of a different $[AlF_6]^{3-}$ octahedron. In turn, each fluoride ligand functions as acceptor for three hydrogen bonds from ammonia ligands of three different $[In(NH_3)_6]^{3+}$ octahedra. The resulting three-dimensional hydrogen bonding system is visualized in Figure 6. The three distinguishable hydrogen bonds feature N···F distances in the narrow range of 296–304

pm (sum of van der Waals radii 302 pm [27]) with ∡(NHF) angles of 160–163°, indicating them quite similar and rather strong. For detailed information on the hydrogen bonds in $[In(NH_3)_6][AlF_6]$, see Table 7.

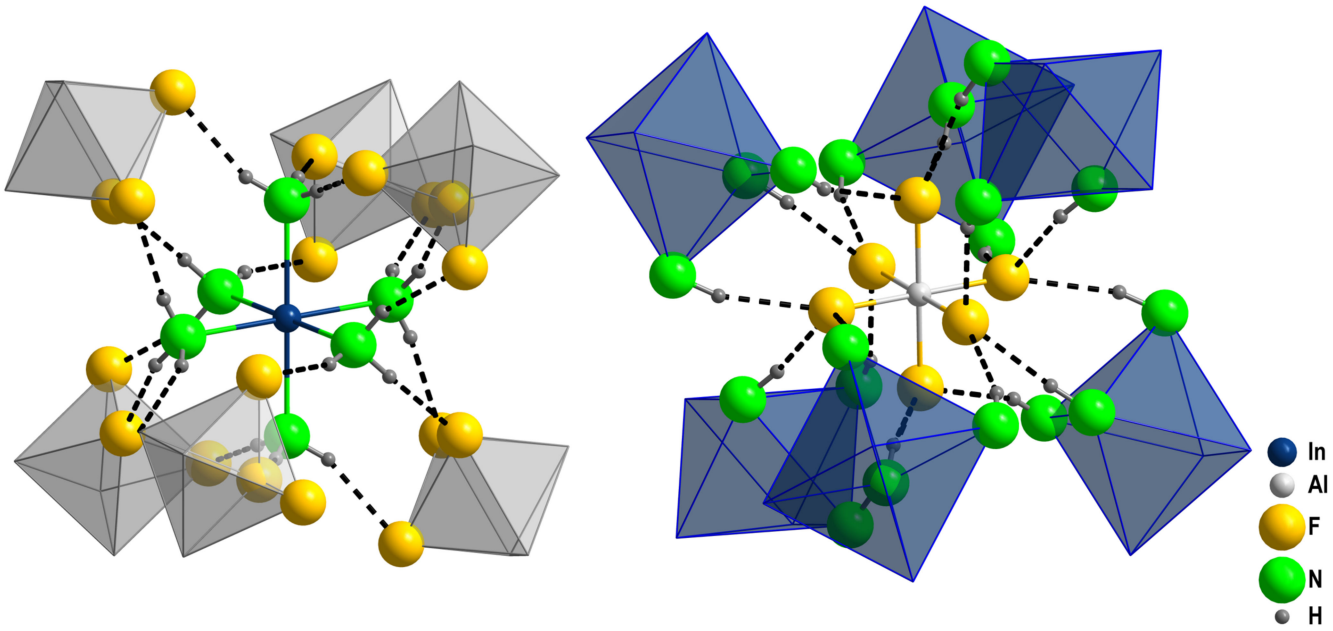

Figure 6. Visualization of the hydrogen bond network in $[In(NH_3)_6][AlF_6]$. Atoms at the outer edges of the octahedra were omitted for clarity.

Table 7. Interatomic distances (in pm) and angles (in deg.) of the hydrogen bonds in $[In(NH_3)_6][AlF_6]$.

	D–H	A	H···A	D···A	∡(DHA)
N–H(1)	94(2)	F	212(2)	303.7(2)	163(2)
N–H(2)	90(2)	F	210(3)	295.7(2)	160(2)
N–H(3)	80(2)	F	220(2)	296.4(2)	160(2)

3.2.2. Vibrational Spectroscopy

Raman and IR spectra of $[In(NH_3)_6][AlF_6]$ are depicted in Figure 7 and the results are summarized in Table 8. The $\nu(NH_3)$ stretching vibrations appear in the range of 3200–3250 cm^{-1} in the Raman spectrum, quite similar to the energy range for these modes in $InAlF_6(NH_3)_2$. Because of the strong hydrogen bonds in $[In(NH_3)_6][AlF_6]$, the stretching vibrations $\nu(NH_3)$ are shifted to lower energies compared to gaseous NH_3 [28]. In the IR spectrum, additional signals for $\nu(NH_3)$ stretching vibrations at 3310 and 3164 cm^{-1} can be observed. In the Raman spectrum, two signals with low intensity are present at 2911 and 2972 cm^{-1} due to Fermi resonance, as has been previously described for similar compounds [35,36]. The $\delta_d(NH_3)$ deformation vibrations can be observed at 1675 cm^{-1} in the Raman spectrum and at 1641 cm^{-1} in the IR spectrum, respectively, in a rather typical energy range. The $\delta_s(NH_3)$ deformation modes present at 1244 cm^{-1} (Raman) and at 1278 and 1255 cm^{-1} (IR). In $[M(NH_3)_6][AlF_6]$ (M = Co, Cr, and Rh), these vibrations are observed at 1312–1346 cm^{-1} [35]. The rocking vibrations can be observed in the IR spectrum at 777 and 685 cm^{-1}, which is at a higher energy compared to those for $[M(NH_3)_6][AlF_6]$ (M = Co, Cr, and Rh). In the Raman spectrum of $[In(NH_3)_6][AlF_6]$ below 550 cm^{-1}, stretching and deformation modes of the complex ions can be observed.

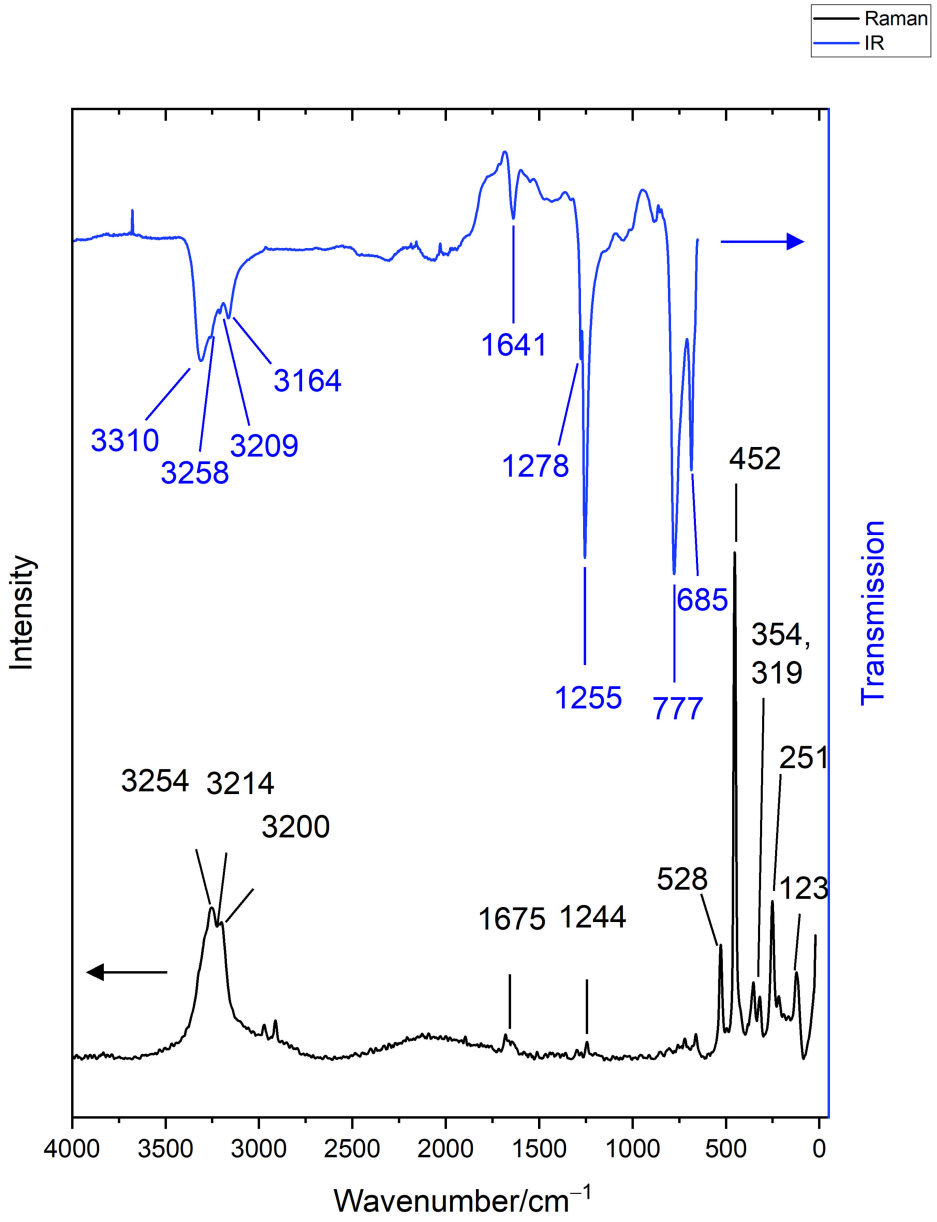

Figure 7. Top: IR spectrum of a powder sample of $[In(NH_3)_6][AlF_6]$; bottom: single crystal Raman spectrum of $[In(NH_3)_6][AlF_6]$, excitation wavelength: 638 nm.

Table 8. Observed vibrations in single crystal Raman spectroscopy and IR spectroscopy (in cm^{-1}) of $[In(NH_3)_6][AlF_6]$.

Vibration Mode	Raman	IR
$\nu(NH_3)$	3253, 3214, 3200	3310, 3258, 3209, 3164
$\delta_d(NH_3)$	1675	1641
$\delta_s(NH_3)$	1244	1278, 1255
$\rho(NH_3)$	–	777, 685
ν(In–N, Al–F), δ(N–In–N, F–Al–F)	123–528	–

3.3. $[In_2F(NH_3)_{10}]_2[SiF_6]_5 \cdot 2\ NH_3$

3.3.1. Crystal Structure

Bis[decaammine-μ-fluoridodiindium (III)] pentakis(hexafluoridosilicate) diammoniate, $[In_2F(NH_3)_{10}]_2[SiF_6]_5 \cdot 2\ NH_3$, crystallizes in the orthorhombic space group *Pnma*. Selected crystallographic data and structure refinement parameters at 100 and 293 K are presented in Table 2, and the fractional atomic coordinates and displacement parameters are given in Tables S3 and S4 in the Supplementary Materials. The crystal structure features 3 crystallographic positions for indium, 3 for silicon, 22 for nitrogen, 32 for fluorine, and 34 for hydrogen. The positions of all hydrogen atoms were taken from the difference Fourier map and refined with isotropic displacement parameters fixed to 1.2 times the isotropic displacement parameter of the adjacent nitrogen atom. For the ammonia molecule not attached to indium (site N(14)), it was not possible to determine the positions of the hydrogen atoms, probably due to rotational disorder. The In–N, In–F, and Si–F distances are presented in Table 9. The In–N distances are in the range of 215–225 pm, which is similar to the In–N distances observed in the other title compounds $InAlF_6(NH_3)_2$ and $[In(NH_3)_6][AlF_6]$, with 214 pm and 224 pm, respectively (see above). Correspondingly, the In–F distances with 213 and 214 pm are similar to those found for $InAlF_6(NH_3)_2$ (212 pm). The Si–F distances are within the range of 160–169 pm. For comparison, Stanko et al. described $[Co(NH_3)_5Cl][SiF_6]$ with Si–F distances of 166–168 pm.

Table 9. Selected interatomic distances in $[In_2F(NH_3)_{10}]_2[SiF_6]_5 \cdot 2\ NH_3$.

	Distance/pm		**Distance/pm**
In(1)–F(1)	214.8(5)	Si(1)–F(3)	160.1(7)
In(1)–N(1)	218.4(8)	Si(1)–F(4)	165.2(5)
In(1)–N(2)	220.8(8)	Si(1)–F(5)	166.3(6)
In(1)–N(3)	223.3(8)	Si(1)–F(6)	166.4(6)
In(1)–N(4)	225.5(6) 2×	Si(1)–F(7)	167.9(6)
In(2)–F(1)	213.4(5)	Si(1)–F(8)	167.7(5)
In(2)–N(5)	222.1(8)	Si(2)–F(9)	167.5(5) 2×
In(2)–N(6)	222.0(8)	Si(2)–F(10)	166.5(8)
In(2)–N(7)	223.0(8)	Si(2)–F(11)	167.0(5) 2×
In(2)–N(8)	224.7(6) 2×	Si(2)–F(12)	164.3(7)
In(3)–F(2)	213.81(4)	Si(3)–F(13)	166.9(4)
In(3)–N(9)	221.7(6)	Si(3)–F(14)	167.8(5)
In(3)–N(10)	222.1(6)	Si(3)–F(15)	168.0(5)
In(3)–N(11)	222.5(6)	Si(3)–F(16)	168.6(4)
In(3)–N(12)	223.9(6)	Si(3)–F(17)	168.3(5)
In(3)–N(13)	224.2(6)	Si(3)–F(18)	169.4(4)

The crystal structure of $[In_2F(NH_3)_{10}]_2[SiF_6]_5 \cdot 2\ NH_3$ features two crystallographic distinguishable octahedra doubles $[(NH_3)_5In(1)–F–In(2)(NH_3)_5]^{5+}$ and $[(NH_3)_5In(3)–F–In(3)(NH_3)_5]^{5+}$ next to three distinct $[SiF_6]^{2-}$ octahedra and the ammonia molecule. The complex ions are depicted in Figure 8.

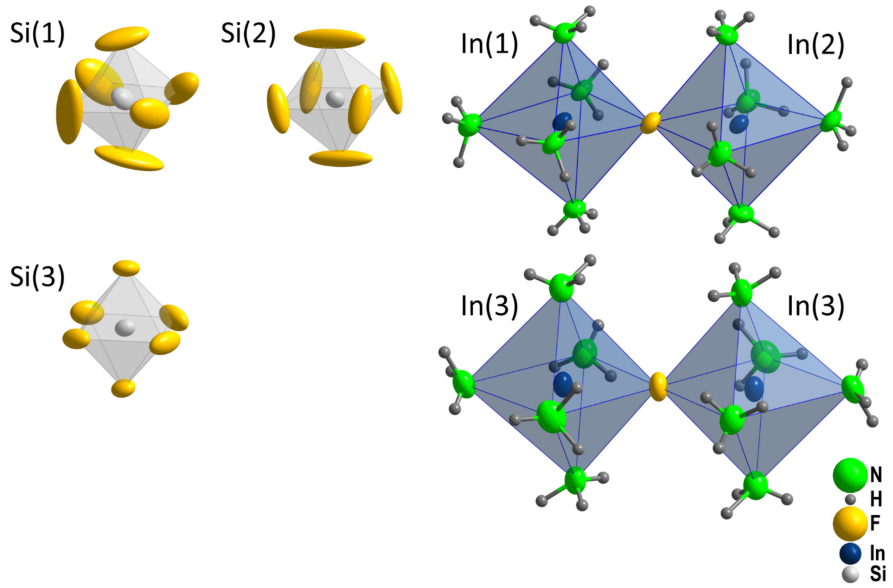

Figure 8. Coordination of the cations in $[In_2F(NH_3)_{10}]_2[SiF_6]_5 \cdot 2\ NH_3$. Atoms are represented by anisotropic displacement ellipsoids (probability of 70%), taken from the refinement of the diffraction data gathered at 100 K.

The interconnection of all constituting ions and the ammoniate molecule is realized by hydrogen bonds (Figure 9). The octahedra double $[(NH_3)_5In(1)–F–In(2)(NH_3)_5]^{5+}$ is surrounded by 12 $[SiF_6]^{2-}$ octahedra, arranged as two face-sharing tetragonal antiprisms centered by In. In contrast, only 10 $[SiF_6]^{2-}$ octahedra constitute the environment of the octahedra double $[(NH_3)_5In(3)–F–In(3)(NH_3)_5]^{5+}$. The environment of the $[Si(1)F_6]^{2-}$ octahedra is fundamentally different from the other two distinct $[SiF_6]^{2-}$ ions, since it carries the ammoniate molecules (Figure 10).

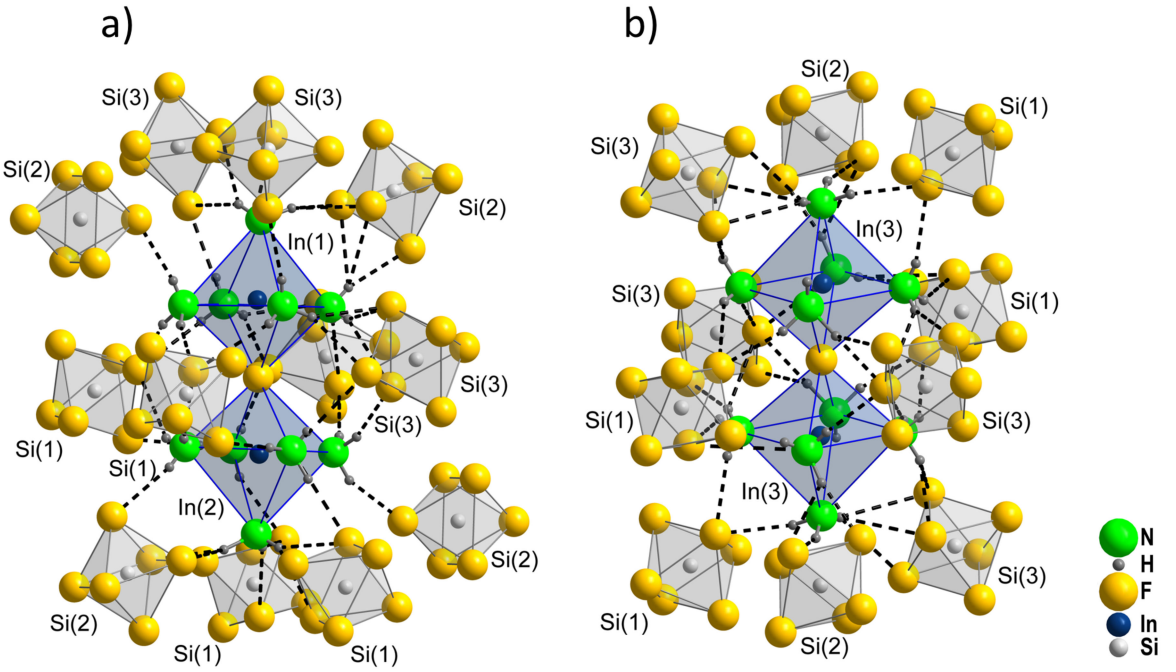

Figure 9. Interconnection of (**a**) the $[(NH_3)_5In(1)–F–In(2)(NH_3)_5]^{5+}$ octahedra double via hydrogen bonds to 12 $[SiF_6]^{2-}$ octahedra and (**b**) the $[(NH_3)_5In(3)–F–In(3)(NH_3)_5]^{5+}$ octahedra double via hydrogen bonds to 10 $[SiF_6]^{2-}$ octahedra.

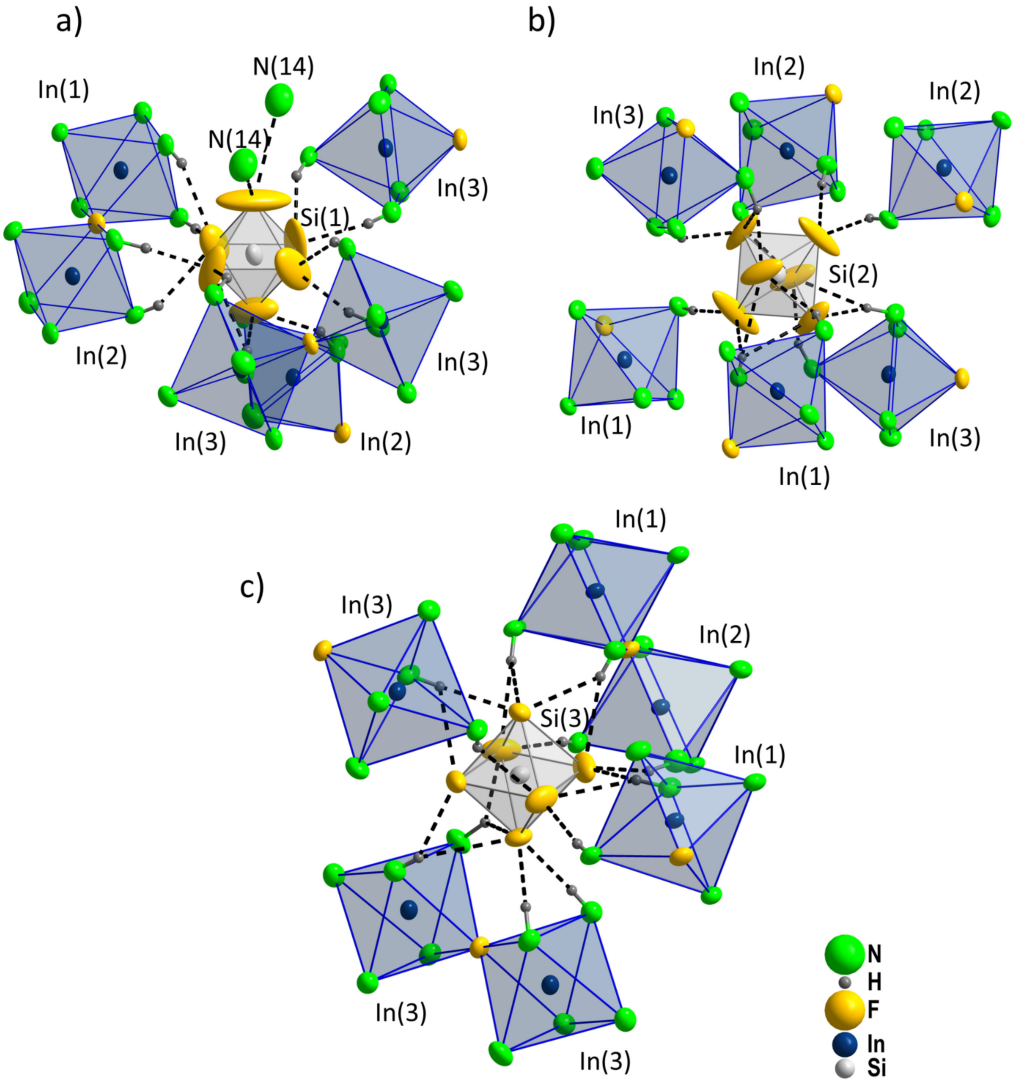

Figure 10. Interconnection of $[SiF_6]^{2-}$ octahedra to $[(NH_3)_5In{-}F{-}In(NH_3)_5]^{5+}$ octahedra doubles via hydrogen bonds for (**a**) $[Si(1)F_6]^{2-}$, (**b**) $[Si(2)F_6]^{2-}$, and (**c**) $[Si(3)F_6]^{2-}$.

$[In_2F(NH_3)_{10}]_2[SiF_6]_5 \cdot 2\,NH_3$ features numerous N–H···F hydrogen bonds. A total of 46 different hydrogen contacts with N···F distances of 276–329 pm and ∡(NHF) angles of 119 to 176° can be observed, which are listed in Table S5 in the Supplementary Materials, together with the relevant distances and angles corresponding to variously strong interactions. Since no hydrogen atoms of the $N(14)H_3$ molecule could be refined, the data for N(14)–H···F hydrogen bonds are incomplete and no statement on their strength can be made. As it can be taken from Figure 11, the ammonia molecule has short distances to fluoride ions of three $[SiF_6]^{2-}$ octahedra with one N(14)···F(3) distance shorter than 302 pm.

With respect to the structure refinement data, especially conspicuous are the large and elongated thermal ellipsoids of the fluorine atoms F(3–12) bound to Si(1) and Si(2) (compare Figure 10). Yet, from the diffraction data, we see no evidence for additional reflections or diffuse scattering, which may point to a superstructure, modulation, or static disorder. However, due to the comparably low scattering power of the affected fluorine atoms, such effects might be hard to observe. Introducing split positions for those fluorine atoms with large thermal ellipsoids failed to improve the crystal structure model. In order to scrutinize thermal oscillation, we have performed a second single crystal diffraction experiment at lower temperature of 100 K using the identical crystal in addition to the initial measurement at 293 K. The averaged displacement parameters U_{11}, U_{22}, U_{33}, and

U_{eq}, respectively, for distinct atom groups (In, Si, N(1–13), ammoniate N(14), F(1) and F(2) bridging In, and F(3–8), F(9–12), F(13–18) of the three distinct $[SiF_6]^{2-}$ octahedra) were plotted against the temperature and extrapolated to 0 K. As it can be taken from Figure 12, nearly all extrapolated lines meet closely at a low common residual displacement parameter at 0 K, except for those for F(3–8) and, particularly, F(9–12), deviating to much larger values. This might indicate a static disorder rather than a thermal displacement as reason for the observed enlarged displacement parameters. An analysis of the main tensor elements U_{ii} is given in Figure S2 and Table S6 in the Supplementary Materials.

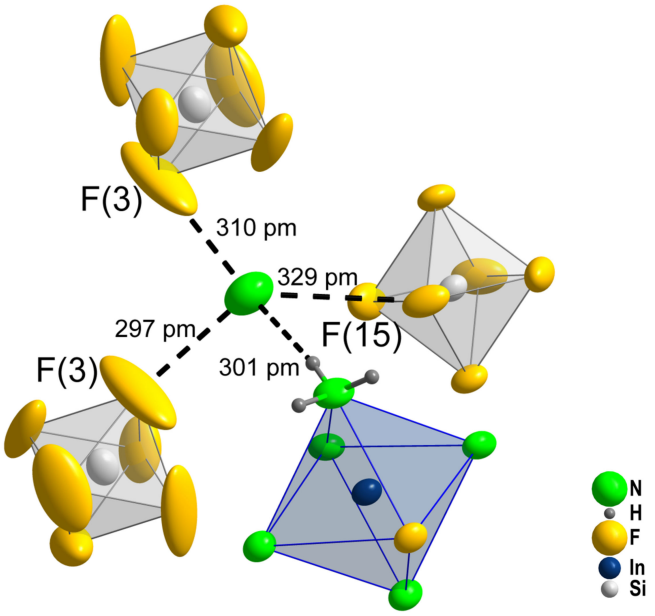

Figure 11. Coordination geometry of the N(14)H_3 molecule together with the N···F bond length of the hydrogen bonds (dashed lines).

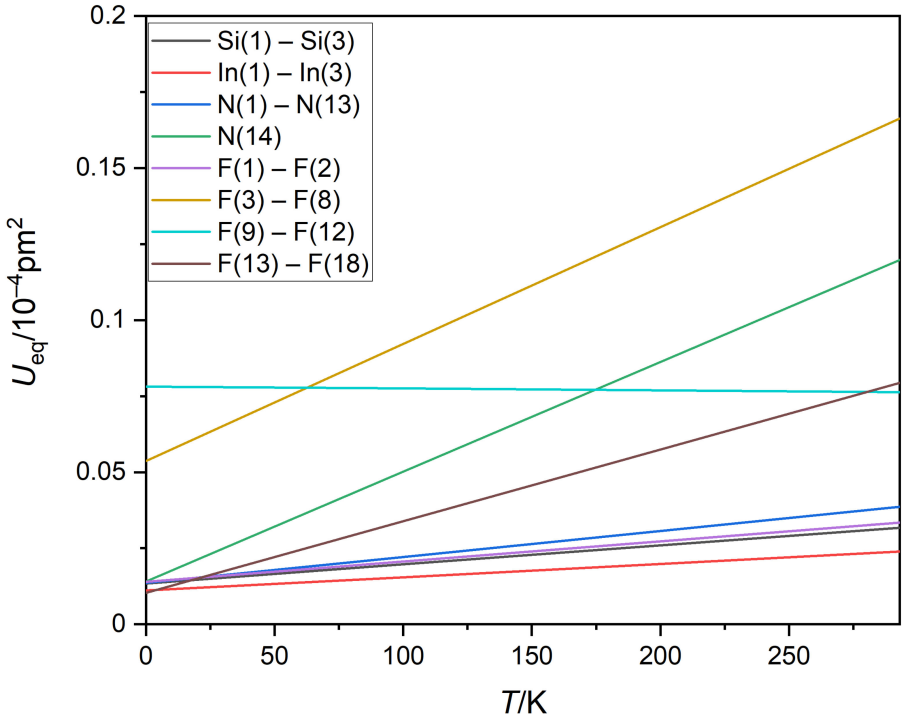

Figure 12. Extrapolation of U_{eq} to 0 K, using data from single crystal diffraction experiments at 293 and 100 K, for the above-mentioned atom groups. The comprehensive extrapolation of U_{11}, U_{22}, U_{33}, and U_{eq} to 0 K can be found in Figure S2 and Table S6 in the Supplementary Materials.

3.3.2. Raman Spectroscopy

The Raman spectrum of $[In_2F(NH_3)_{10}]_2[SiF_6]_5 \cdot 2\ NH_3$ recorded on a single crystal is shown in Figure 13, the energies of the vibration modes are gathered in Table 10. The $\nu(NH_3)$ stretching vibrations can be observed as one intense, broadened signal at 3231 cm^{-1}. The broadening of this signal arises probably as an overlap of multiple signals combined with the presence of multiple hydrogen bonds differing in their strength and thus, shifted to different wavenumbers. The energy of the signal maximum presents quite similar to stretching vibrations observed in $[In(NH_3)_5Cl]Cl_2$, $[In(NH_3)_6]I_3 \cdot NH_3$, $InAlF_6(NH_3)_2$, and $[In(NH_3)_6][AlF_6]$ [18,20].

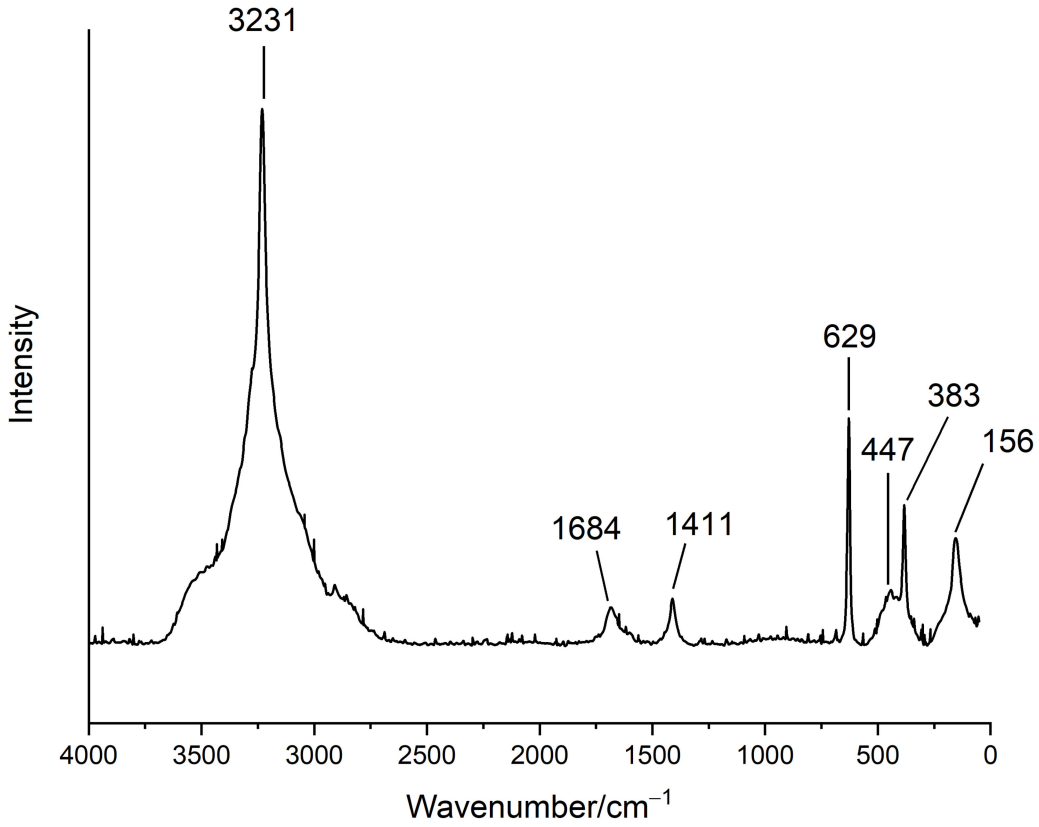

Figure 13. Single crystal Raman spectrum of $[In_2F(NH_3)_{10}]_2[SiF_6]_5 \cdot 2\ NH_3$, excitation energy: 532 nm.

Table 10. Comparison of the observed Raman modes of $[In_2F(NH_3)_{10}]_2[SiF_6]_5 \cdot 2\ NH_3$ and $(NH_4)_2[SiF_6]$ in cm^{-1} [40].

Vibration Mode	$[In_2F(NH_3)_{10}]_2[SiF_6]_5 \cdot 2\ NH_3$	Vibration Mode	$(NH_4)_2[SiF_6]$
$\nu(NH_3)$	3231	$\nu(NH_4)$	3200–3350
$\delta_d(NH_3)$	1684	$\delta_d(NH_4)$	1700
$\delta_s(NH_3)$	1411	$\delta_s(NH_4)$	1408, 1420, 1450
ν(Si–F), δ(F–Si–F) ν(In–F,N), δ(N–In–N,F)	629, 447, 383, 156	ν(Si–F), δ(F–Si–F)	656, 468, 400, 148

The symmetric and antisymmetric deformation vibration can be observed at higher wavenumbers ($\delta_d(NH_3)$ = 1684 cm^{-1}, $\delta_s(NH_3)$ = 1411 cm^{-1}) compared to other metal ammine complexes ($\delta_d(NH_3)$ = 1570–1650 cm^{-1}, $\delta_s(NH_3)$ = 1158–1355 cm^{-1}) and the above discussed indium ammoniates [41], however they are quite similar to those observed for $(NH_4)_2[SiF_6]$ (compare Table 10) [40]. The $\rho(NH_3)$ rocking vibrations would be expected

around 750 cm^{-1}, but are too low in intensity for a reliable assignment. The Si–F, In–F, and In–N stretching vibrations, as well as the F−Si−F and F–In–F,N deformation modes are found in the range of 156 to 629 cm^{-1}.

4. Conclusions

Three solid intermediates in the systems In/Al and In/Si were obtained from near-ammononeutral conditions, similar to those utilized for InN synthesis: $InAlF_6(NH_3)_2$, $[In(NH_3)_6][AlF_6]$, and $[In_2F(NH_3)_{10}]_2[SiF_6]_5 \cdot 2\ NH_3$. These three intermediates are the first known indium ammoniates containing aluminum and silicon, respectively. All three compounds can be considered as corrosion products of the liner material Si_3N_4, which contains small amounts of aluminum. So far, the dissolution of cations from the liner material has only been observed in experiments where InF_3 is used as indium source. All three compounds show a retrograde solubility within the applied temperature range, as is similarly known for $InF_2(NH_2)$, indicating a lower solubility at higher temperatures within the applied range of synthetic conditions. The crystal structures of $[In(NH_3)_6][AlF_6]$ and $[In_2F(NH_3)_{10}]_2[SiF_6]_5 \cdot 2\ NH_3$ feature isolated molecules and complex ions, interconnected via hydrogen bonds, while $InAlF_6(NH_3)_2$ crystallizes as a layer-type structure. With these three solid intermediates, we present evidence for the participation of aluminum and silicon cations in the ammonothermal crystal growth of InN, using Si_3N_4 liners and InF_3 as a starting material.

Supplementary Materials: The following are available online at https://www.mdpi.com/article/10.3390/cryst11060679/s1. All relevant powder patterns, anisotropic displacement parameters of the single crystal refinements, the atomic coordinates, and isotropic displacement parameters of $[In_2F(NH_3)_{10}]_2[SiF_6]_5 \cdot 2\ NH_3$, as well as the comprehensive extrapolations of the displacement parameters for $[In_2F(NH_3)_{10}]_2[SiF_6]_5 \cdot 2\ NH_3$, can be found in the supporting information. The following data are available online at https://www.mdpi.com/article/10.3390/cryst11060679/s1. Figure S1: X-ray powder pattern of $[In(NH_3)_6][AlF_6]$; Figure S2: Extrapolation of U_{11}, U_{22}, U_{33}, and U_{eq} to 0 K; Table S1: Anisotropic displacement parameters in 10^4 pm^2 of $InAlF_6(NH_3)_2$; Table S2: Anisotropic displacement parameters in 10^4 pm^2 of $[In(NH_3)_6][AlF_6]$; Table S3: Atomic coordinates and isotropic displacement parameters in 10^4 pm^2 of $[In_2F(NH_3)_{10}]_2[SiF_6]_5 \cdot 2\ NH_3$; Table S4: Anisotropic displacement parameters U_{ij} in 10^4 pm^2 of $[In_2F(NH_3)_{10}]_2[SiF_6]_5 \cdot 2\ NH_3$; Table S5: Selected interatomic distance in pm and angles in degree of the hydrogen bonds in $[In_2F(NH_3)_{10}]_2[SiF_6]_5 \cdot 2\ NH_3$; Table S1**:** Extrapolation of U_{11}, U_{22}, U_{33} and U_{eq} for $[In_2F(NH_3)_{10}]_2[SiF_6]_5 \cdot 2\ NH_3$ to 0 K. Further details of the crystal structure investigations may be obtained from the Fachinformationszentrum Karlsruhe, D-76344 Eggenstein-Leopoldshafen, Germany, on quoting the depository numbers CSD-2082107 for $InAlF_6(NH_3)_2$, CSD-2082120 for $[In(NH_3)_6][AlF_6]$, CSD-2082089 for $[In_2F(NH_3)_{10}]_2[SiF_6]_5 \cdot 2\ NH_3$ measured at 100 K, and CSD-2082092 for $[In_2F(NH_3)_{10}]_2[SiF_6]_5 \cdot 2\ NH_3$ measured at 293 K.

Author Contributions: Conceptualization, P.B. and R.N.; methodology, P.B. and T.B.C.; formal analysis, P.B. and T.B.C.; investigation, P.B. and T.B.C.; resources, R.N.; data curation, P.B. and T.B.C.; writing—original draft preparation, P.B. and R.N.; writing—review and editing, P.B. and R.N.; visualization, P.B.; supervision, R.N.; project administration, R.N.; funding acquisition, R.N. All authors have read and agreed to the published version of the manuscript.

Funding: This research was funded by the Deutsche Forschungsgemeinschaft (DFG), grant number NI489/16-1.

Acknowledgments: We want to thank Falk Lissner for conducting the single crystal diffraction experiments and Sebastian Kunkel, Kevin Bareiß, and Florian Goerigk for conducting the vibrational spectroscopy.

Conflicts of Interest: The authors declare no conflict of interest.

References

1. DenBaars, S.P.; Feezell, D.; Kelchner, K.; Pimputkar, S.; Pan, C.-C.; Yen, C.-C.; Tanaka, S.; Zhao, Y.; Pfaff, N.; Farrell, R.; et al. Development of gallium-nitride-based light-emitting diodes (LEDs) and laser diodes for energy-efficient lighting and displays. *Acta Mater.* **2013**, *61*, 945–951. [CrossRef]

2. Perry, P.B.; Rutz, R.F. The optical absorption edge of single-crystal AlN prepared by a close-spaced vapor process. *Appl. Phys. Lett.* **1978**, *33*, 319–321. [CrossRef]
3. Maruska, H.P.; Tietjen, J.J. The Preparation and properties of vapor-deposited single-crystalline GaN. *Appl. Phys. Lett.* **1969**, *15*, 327–329. [CrossRef]
4. Wu, J.; Walukiewicz, W.; Yu, K.M.; Ager, J.W.; Haller, E.E.; Lu, H.; Schaff, W.J.; Saito, Y.; Nanishi, Y. Unusual properties of the fundamental band gap of InN. *Appl. Phys. Lett.* **2002**, *80*, 3967–3969. [CrossRef]
5. Davydov, V.Y.; Klochikhin, A.A.; Seisyan, R.P.; Emtsev, V.V.; Ivanov, S.V.; Bechstedt, F.; Furthmller, J.; Harima, H.; Mudryi, A.V.; Aderhold, J.; et al. Absorption and Emission of Hexagonal InN. Evidence of Narrow Fundamental Band Gap. *Phys. Status Solidi B* **2002**, *229*, R1–R3. [CrossRef]
6. Tansley, T.L.; Foley, C.P. Optical band gap of indium nitride. *J. Appl. Phys.* **1986**, *59*, 3241–3244. [CrossRef]
7. Technology of Gallium Nitride Crystal Growth. In *Springer Series in Materials Science*; Ehrentraut, D.; Bockowski, M.; Meissner, E. (Eds.) Springer-Verlag: Berlin/Heidelberg, Germany, 2010; ISBN 978-3-642-04830-2.
8. Häusler, J.; Schnick, W. Ammonothermal Synthesis of Nitrides: Recent Developments and Future Perspectives. *Chem. Eur. J.* **2018**, *24*, 11864–11879. [CrossRef] [PubMed]
9. Richter, T.M.M.; Niewa, R. Chemistry of Ammonothermal Synthesis. *Inorganics* **2014**, *2*, 29–78. [CrossRef]
10. Ammonothermal Synthesis and Crystal Growth of Nitrides. In *Springer Series in Materials Science*; Meissner, E.; Niewa, R. (Eds.) Springer International Publishing: Cham, Germany, 2021; ISBN 978-3-030-56304-2.
11. Bockowski, M.; Iwinska, M.; Amilusik, M.; Fijalkowski, M.; Lucznik, B.; Sochacki, T. Challenges and future perspectives in HVPE-GaN growth on ammonothermal GaN seeds. *Semicond. Sci. Technol.* **2016**, *31*, 93002. [CrossRef]
12. Ranade, M.R.; Tessier, F.; Navrotsky, A.; Marchand, R. Calorimetric determination of the enthalpy of formation of InN and comparison with AlN and GaN. *J. Mater. Res.* **2001**, *16*, 2824–2831. [CrossRef]
13. Hertrampf, J.; Becker, P.; Widenmeyer, M.; Weidenkaff, A.; Schlücker, E.; Niewa, R. Ammonothermal Crystal Growth of Indium Nitride. *Cryst. Growth Des.* **2018**, *18*, 2365–2369. [CrossRef]
14. Hertweck, B.; Schimmel, S.; Steigerwald, T.G.; Alt, N.S.A.; Wellmann, P.J.; Schluecker, E. Ceramic liner technology for ammonoacidic synthesis. *J. Supercrit. Fluids* **2015**, *99*, 76–87. [CrossRef]
15. Purdy, A.P. Indium(III) amides and nitrides. *Inorg. Chem.* **1994**, *33*, 282–286. [CrossRef]
16. Ketchum, D.R.; Schimek, G.L.; Pennington, W.T.; Kolis, J.W. Synthesis of new Group III fluoride–ammonia adducts in supercritical ammonia: Structures of $AlF_3(NH_3)_2$ and $InF_2(NH_2)(NH_3)$. *Inorg. Chim. Acta* **1999**, *294*, 200–206. [CrossRef]
17. Bremm, S.; Meyer, G. Triamminetrichloroindium(III), $[InCl_3(NH_3)_3]$. *Acta Cryst. E* **2003**, *59*, i110–i111. [CrossRef]
18. Becker, P.; Cekovski, T.B.; Niewa, R. Two Intermediates in Ammonothermal InN Crystal Growth: $[In(NH_3)_5Cl]Cl_2$ and $InF_2(NH_2)$. *Z. Anorg. Allg. Chem.* **2021**, in press. [CrossRef]
19. Alt, N.S.A.; Meissner, E.; Schluecker, E. Development of a novel in situ monitoring technology for ammonothermal reactors. *J. Cryst. Growth* **2012**, *350*, 2–4. [CrossRef]
20. Zhang, S. *Intermediates During the Formation of GaN Under Ammonothermal Conditions*; Dr. Hut: München, Germany, 2014; ISBN 9783843917957.
21. Hüttig, G.F. Apparat zur gleichzeitigen Druck- und Raummessung von Gasen. (Tensi-Eudiometer.). *Z. Anorg. Allg. Chem.* **1920**, *114*, 161–173. [CrossRef]
22. Erlekampf, J.; Seebeck, J.; Savva, P.; Meissner, E.; Friedrich, J.; Alt, N.S.A.; Schlücker, E.; Frey, L. Numerical time-dependent 3D simulation of flow pattern and heat distribution in an ammonothermal system with various baffle shapes. *J. Cryst. Growth* **2014**, *403*, 96–104. [CrossRef]
23. Schimmel, S.; Tomida, D.; Ishiguro, T.; Honda, Y.; Chichibu, S.; Amano, H. Numerical Simulation of Ammonothermal Crystal Growth of GaN—Current State, Challenges, and Prospects. *Crystals* **2021**, *11*, 356. [CrossRef]
24. Sheldrick, G.M. Crystal structure refinement with SHELXL. *Acta Cryst. C* **2015**, *71*, 3–8. [CrossRef]
25. Sheldrick, G.M. A short history of SHELX. *Acta Cryst. A* **2008**, *64*, 112–122. [CrossRef] [PubMed]
26. June Sutor, D. The C–H . . . O Hydrogen Bond in Crystals. *Nature* **1962**, *195*, 68–69. [CrossRef]
27. Bondi, A. van der Waals Volumes and Radii. *J. Phys. Chem.* **1964**, *68*, 441–451. [CrossRef]
28. Svatos, G.F.; Curran, C.; Quagliano, J.V. Infrared Absorption Spectra of Inorganic Coordination Complexes. The N–H Stretching Vibration in Coordination Compounds. *J. Am. Chem. Soc.* **1955**, *77*, 6159–6163. [CrossRef]
29. Roos, M.; Meyer, G. Das Monoammoniakat des Galliumamidfluorids: $Ga(NH_3)(NH_2)F_2$. *Z. Anorg. Allg. Chem.* **1999**, *625*, 1839–1842. [CrossRef]
30. Jacobs, H.; Schröder, F.O. Penta-Ammoniates of Aluminium Halides: The Crystal Structures of $AlX_3 \cdot 5NH_3$ with X. = Cl, Br, I.Z. *Anorg. Allg. Chem.* **2002**, *628*, 951–955. [CrossRef]
31. Bremm, S.; Meyer, G. Metallampullen als Mini-Autoklaven: Synthese und Kristallstrukturen der Ammoniakate $[Al(NH_3)_4Cl_2][Al(NH_3)_2Cl_4]$ und $(NH_4)_2[Al(NH_3)_4Cl_2][Al(NH_3)_2Cl_4]Cl_2$. *Z. Anorg. Allg. Chem.* **2001**, *627*, 407–410. [CrossRef]
32. Jacobs, H.; Schröder, F.O. Monoammoniates of Aluminium Halides: The Crystal Structures of $AlBr_3 \cdot NH_3$ and $AlI_3 \cdot NH_3$. *Z. Anorg. Allg. Chem.* **2002**, *628*, 327–329. [CrossRef]
33. Peters, D.; Bock, J.; Jacobs, H. Hexaaminaluminiumiodidmonoammoniakat—$[Al(NH_3)_6]I_3NH_3$—Darstellung und Kristallstruktur. *J. Less-Common Met.* **1989**, *154*, 243–250. [CrossRef]

34. Zhang, S.; Hintze, F.; Schnick, W.; Niewa, R. Intermediates in Ammonothermal GaN Crystal Growth under Ammonoacidic Conditions. *Eur. J. Inorg. Chem.* **2013**, *2013*, 5387–5399. [CrossRef]
35. Wieghardt, K.; Siebert, H. Schwingungsspektren und Kristallgitter von Hexamminchrom(III)- und Hexamminkobalt(III)-hexafluoro-metallaten(III). *J. Mol. Struct.* **1971**, *7*, 305–313. [CrossRef]
36. Wieghardt, K.; Siebert, H. Zur Kenntnis der Hexafluoromanganate(III). *Z. Anorg. Allg. Chem.* **1971**, *381*, 12–20. [CrossRef]
37. Wieghardt, K.; Weiss, J. Die Kristallstrukturen von Hexamminchrom(III)-Hexafluoromanganat(III) und Hexamminchrom(III)-Hexafluoroferrat(III). *Acta Cryst. B* **1972**, *28*, 529–534. [CrossRef]
38. Subramanian, M.A.; Harlow, R.H.; Rao, V.N.M. New $[Ru(NH_3)_6]MF_6$ phases: Precursors to catalysts for halogenation reactions. *Mater. Res. Bull.* **2000**, *35*, 1587–1592. [CrossRef]
39. Shannon, R.D. Revised Effective Ionic Radii and Systematic Studies of Interatomic Distances in Halides and Chalcogenides. *Acta Cryst.* **1976**, *A32*, 751–767. [CrossRef]
40. Poulet, H.; Mathieu, J.P. Raman spectroscopic studies of the various phases of crystalline ammonium fluosilicate $(NH_4)_2SiF_6$. *J. Raman Spectrosc.* **1976**, *5*, 193–198. [CrossRef]
41. Svatos, G.F.; Sweeny, D.M.; Mizushima, S.-I.; Curran, C.; Quagliano, J.V. Infrared Absorption Spectra of Inorganic Coordination Complexes. 1a,b XII. The Characteristic NH_3 Deformation Vibrations of Solid Inorganic Complexes. *J. Am. Chem. Soc.* **1957**, *79*, 3313–3315. [CrossRef]